

# Multigrid Waveform Relaxation for Anisotropic Partial Differential Equations

*Jan Van lent*  
*Stefan Vandewalle*

*Report TW 320, February 2001*



Katholieke Universiteit Leuven  
Department of Computer Science  
Celestijnenlaan 200A – B-3001 Heverlee (Belgium)

# Multigrid Waveform Relaxation for Anisotropic Partial Differential Equations

*Jan Van lent*  
*Stefan Vandewalle*

*Report TW 320, February 2001*

Department of Computer Science, K.U.Leuven

## **Abstract**

Multigrid waveform relaxation provides fast iterative methods for the solution of time-dependent partial differential equations. In this paper we consider anisotropic problems and extend multigrid methods developed for the stationary elliptic case to waveform relaxation methods for the time-dependent parabolic case. We study line-relaxation, semicoarsening and multiple semicoarsening multi-level methods. A two-grid Fourier-Laplace analysis is used to estimate the convergence of these methods for the rotated anisotropic diffusion equation. We treat both continuous time and discrete time algorithms. The results of the analysis are confirmed by numerical experiments.

**Keywords :** Waveform Relaxation, Multigrid, Anisotropic Problems, Parabolic Partial Differential Equations

**AMS(MOS) Classification :** Primary : 65M55, Secondary : 65M20.

# Multigrid Waveform Relaxation for Anisotropic Partial Differential Equations

Jan Van lent and Stefan Vandewalle\*  
{jan.vanlent,stefan.vandewalle}@cs.kuleuven.ac.be  
K.U.Leuven, Dept. of Computer Science,  
Celestijnenlaan 200A, B-3001 Heverlee, Belgium

## 1 Introduction

Waveform relaxation is an iterative method for solving systems of ODEs. It was first studied as a practical solution method in the context of integrated circuit simulation by Lelarsmee et al. [6]. For an overview of waveform relaxation developments we refer to [1]. The convergence of waveform relaxation for linear systems of ODEs was studied by Miekka and Nevanlinna in [9]. From their analysis one may conclude that the standard waveform relaxation methods show poor convergence when applied to the discretised parabolic diffusion equation. The classical model problem, that is the isotropic, constant coefficient one- or two-dimensional heat equation, can be solved efficiently by multigrid acceleration of the waveform relaxation method, as studied in [7, 12, 2, 13, 10].

The use of the multigrid waveform relaxation method has not yet been studied for solving anisotropic, variable coefficient parabolic problems. In the stationary case standard multigrid waveform relaxation methods brake down when applied to anisotropic problems. Several optimised methods have been proposed to handle stationary anisotropic problems (see [11]). In this paper we study the extension of these methods to time-dependent parabolic problems. We use the time-dependent rotated anisotropic diffusion equation as a test equation.

The paper is organised as follows. Section 2 introduces the model problem and the single-grid and multigrid waveform relaxation methods. Line relaxation, semicoarsening and multiple semicoarsening are proposed as methods for anisotropic problems. In section 3 it is shown how the two-grid local mode Fourier analysis used for stationary multigrid, is extended to multigrid waveform relaxation. The results of the analysis are compared to numerical results in section 4. We end in section 5 with some concluding remarks.

---

\*Corresponding author

## 2 Waveform Relaxation Methods

### 2.1 The Model Problem and Its Discretisation

The waveform relaxation method can be used as a method to approximate solutions of time-dependent parabolic PDEs of the form

$$\frac{\partial \mathbf{u}}{\partial t} = \mathcal{L}\mathbf{u} + \mathbf{f}, \quad (1)$$

with  $\mathcal{L}$  an elliptic operator and with  $\mathbf{u}(t, q)$ ,  $\mathbf{f}(t, q) \in \mathbb{R}$  functions of time  $t \in \Omega_t$  and a spatial coordinate  $q \in \Omega$ . The time interval can be bounded,  $\Omega_t = [0, T]$  or unbounded,  $\Omega_t = [0, \infty)$ . This equation is supplemented with boundary conditions and either an initial condition specifying the solution at  $t = 0$  or a time-periodicity condition of the form  $\mathbf{u}(t, q) = \mathbf{u}(t + T, q)$ .

We will use the rotated anisotropic diffusion equation as a test equation for the numerical methods considered in this paper. This equation is a standard test case for the study of iterative methods [17]. It has two parameters  $\varepsilon$  and  $\beta$ , and is of the form (1) with

$$\mathcal{L} = (\varepsilon c^2 + s^2) \frac{\partial^2}{\partial x^2} + (c^2 + \varepsilon s^2) \frac{\partial^2}{\partial y^2} + 2(\varepsilon - 1)cs \frac{\partial^2}{\partial x \partial y}, \quad (2)$$

where  $c = \cos \beta$  and  $s = \sin \beta$ . The angle  $\beta$  indicates the direction of the anisotropy and  $\varepsilon$  its strength. We consider the initial value problem, defined on the unit square  $\Omega = [0, 1]^2$  with Dirichlet boundary conditions.

The solution is approximated on a rectangular equidistant grid with  $(N_x + 1)(N_y + 1)$  grid points,

$$\begin{aligned} q_{i,j} &= (ih_x, jh_y) \in \Omega, \quad 0 \leq i \leq N_x, \quad 0 \leq j \leq N_y, \\ h &= (h_x, h_y) = (N_x^{-1}, N_y^{-1}). \end{aligned} \quad (3)$$

Let  $u$  and  $f$  denote grids of functions defined by

$$u_{i,j}(t) = u(t, q_{i,j}) \quad \text{and} \quad f_{i,j}(t) = f(t, q_{i,j}). \quad (4)$$

We can now replace the spatial derivatives in the operator  $\mathcal{L}$  by their finite difference approximations. This results in a linear system of ODEs

$$\dot{u} = Lu + f. \quad (5)$$

In particular, for the rotated anisotropic diffusion equation, the discretised differential operator becomes

$$L = \begin{bmatrix} -\frac{(\varepsilon-1)cs}{2h_x h_y} & \frac{c^2 + \varepsilon s^2}{h_y^2} & \frac{(\varepsilon-1)cs}{2h_x h_y} \\ \frac{\varepsilon c^2 + s^2}{h_x^2} & -2\frac{\varepsilon c^2 + s^2}{h_x^2} - 2\frac{c^2 + \varepsilon s^2}{h_y^2} & \frac{\varepsilon c^2 + s^2}{h_x^2} \\ \frac{(\varepsilon-1)cs}{2h_x h_y} & \frac{c^2 + \varepsilon s^2}{h_y^2} & -\frac{(\varepsilon-1)cs}{2h_x h_y} \end{bmatrix}. \quad (6)$$

## 2.2 Single-Grid Waveform Relaxation Methods

### 2.2.1 Continuous Time Iteration Methods

The classical waveform relaxation methods are iterative methods based on a splitting  $L = L^+ + L^-$ , and defined as

$$\dot{u}^{(\nu+1)} = L^+ u^{(\nu+1)} + L^- u^{(\nu)} + f. \quad (7)$$

The splitting is selected in such a way that (7) is easier to solve than the original system, and the successive approximations  $u^{(\nu)}$  converge to the solution of (5). The waveform relaxation variants of some well known iterative schemes are illustrated below for a general nine-point stencil discretisation. Non-zero values in the stencils (taken from the original stencil) are indicated by “•”. For each method a set of  $(N_x - 1)(N_y - 1)$  scalar ODEs of the form  $\dot{y} = py + q$  has to be solved repeatedly.

#### Jacobi

- for all  $(i, j)$ , solve

$$\dot{u}_{i,j}^{(\nu+1)} = [\bullet] u_{i,j}^{(\nu+1)} + \begin{bmatrix} \bullet & \bullet & \bullet \\ \bullet & & \bullet \\ \bullet & \bullet & \bullet \end{bmatrix} u_{i,j}^{(\nu)} + f_{i,j}$$

#### Lexicographic Gauss-Seidel

- for  $j = 1, \dots, N_y - 1$   
for  $i = 1, \dots, N_x - 1$ , solve

$$\dot{u}_{i,j}^{(\nu+1)} = [\bullet] u_{i,j}^{(\nu+1)} + \begin{bmatrix} \bullet & & & \\ \bullet & & & \\ \bullet & \bullet & \bullet & \\ \bullet & \bullet & \bullet & \end{bmatrix} u_{i,j}^{(\nu+1)} + \begin{bmatrix} \bullet & \bullet & \bullet \\ & & \bullet \\ & & \bullet \end{bmatrix} u_{i,j}^{(\nu)} + f_{i,j}$$

#### Red-Black Gauss-Seidel (five-point stencil)

- for all  $(i, j)$  with  $i + j$  even, solve

$$\dot{u}_{i,j}^{(\nu+1)} = [\bullet] u_{i,j}^{(\nu+1)} + \begin{bmatrix} & \bullet & \\ \bullet & & \bullet \\ & \bullet & \end{bmatrix} u_{i,j}^{(\nu)} + f_{i,j}$$

- for all  $(i, j)$  with  $i + j$  odd, solve

$$\dot{u}_{i,j}^{(\nu+1)} = [\bullet] u_{i,j}^{(\nu+1)} + \begin{bmatrix} & \bullet & \\ \bullet & & \bullet \\ & \bullet & \end{bmatrix} u_{i,j}^{(\nu+1)} + f_{i,j}$$

#### Four-Colour Gauss-Seidel

- for all  $(i, j)$  with  $i$  odd,  $j$  odd, solve

$$\dot{u}_{i,j}^{(\nu+1)} = [\bullet] u_{i,j}^{(\nu+1)} + \begin{bmatrix} \bullet & \bullet & \bullet \\ \bullet & & \bullet \\ \bullet & \bullet & \bullet \end{bmatrix} u_{i,j}^{(\nu)} + f_{i,j}$$

- for all  $(i, j)$  with  $i$  even,  $j$  even, solve

$$\dot{u}_{i,j}^{(\nu+1)} = [\bullet] u_{i,j}^{(\nu+1)} + \begin{bmatrix} \bullet & \bullet \\ \bullet & \bullet \end{bmatrix} u_{i,j}^{(\nu+1)} + \begin{bmatrix} \bullet & \bullet \\ \bullet & \bullet \end{bmatrix} u_{i,j}^{(\nu)} + f_{i,j}$$

- for all  $(i, j)$  with  $i$  even,  $j$  odd, solve

$$\dot{u}_{i,j}^{(\nu+1)} = [\bullet] u_{i,j}^{(\nu+1)} + \begin{bmatrix} \bullet & \bullet \\ \bullet & \bullet \end{bmatrix} u_{i,j}^{(\nu+1)} + \begin{bmatrix} \bullet & \bullet \\ \bullet & \bullet \end{bmatrix} u_{i,j}^{(\nu)} + f_{i,j}$$

- for all  $(i, j)$  with  $i$  odd,  $j$  even, solve

$$\dot{u}_{i,j}^{(\nu+1)} = [\bullet] u_{i,j}^{(\nu+1)} + \begin{bmatrix} \bullet & \bullet & \bullet \\ \bullet & \bullet & \bullet \\ \bullet & \bullet & \bullet \end{bmatrix} u_{i,j}^{(\nu+1)} + f_{i,j}$$

Instead of considering subsystems of only one equation, one can also take the set of ODEs on a line of the grid as the subsystems. The horizontal zebra Gauss-Seidel method corresponds to the following series of computations :

### Horizontal Zebra Gauss-Seidel

- for all  $j$  odd, solve

$$\dot{u}_{i,j}^{(\nu+1)} = [\bullet \bullet \bullet] u_{i,j}^{(\nu+1)} + \begin{bmatrix} \bullet & \bullet & \bullet \\ \bullet & \bullet & \bullet \end{bmatrix} u_{i,j}^{(\nu)} + f_{i,j}, \quad 0 < i < N_x$$

- for all  $j$  even, solve

$$\dot{u}_{i,j}^{(\nu+1)} = [\bullet \bullet \bullet] u_{i,j}^{(\nu+1)} + \begin{bmatrix} \bullet & \bullet & \bullet \\ \bullet & \bullet & \bullet \end{bmatrix} u_{i,j}^{(\nu+1)} + f_{i,j}, \quad 0 < i < N_x$$

In that case the equations describe a set of  $N_y - 1$  systems of ODEs of the form  $\dot{y} = Py + q$  with  $P$  tridiagonal. Similarly, one can define the vertical zebra Gauss-Seidel method. The so-called alternating zebra Gauss-Seidel method consists of one horizontal zebra step, followed by one vertical zebra step. These more complicated methods will turn out to be useful to handle anisotropic problems.

### 2.2.2 Discrete Time Iteration Methods

The continuous time waveform relaxation methods operate on grids of continuous functions. In an actual implementation, however, the solutions of the ODEs have to be approximated numerically by means of a time-discretisation. The system resulting from the discretisation of a parabolic PDE is stiff, necessitating the use of implicit solvers. All the standard methods like LMF (BDF), multistage (RK) and multivalued methods can be used, and have been considered in the waveform relaxation literature, see [1] for an overview. We restrict ourselves here to the implicit Euler method with a constant step length. The time points become

$$t_k = kh_t, \quad 0 \leq k \leq N_t, \quad h_t = N_t^{-1}. \quad (8)$$

The numerical solution is now represented by an  $(N_x + 1)(N_y + 1)$  grid of discrete functions

$$u_{i,j} = \{u_{i,j}(t_k)\}_{0 \leq k \leq N_t}. \quad (9)$$

The problem solved by the discrete time iteration can be interpreted as a system of recurrence relations defined on a 2D grid with discrete functions as unknowns, or it can be interpreted as a system of algebraic equations with scalar unknowns defined on a 3D space-time grid.

## 2.3 Multigrid Waveform Relaxation Methods

### 2.3.1 The Multigrid Algorithm

The standard point-wise and line-wise single-grid waveform relaxation techniques turn out to be too slowly convergent for use on fine grids. Like in the elliptic case, this can be resolved by resorting to the use of multigrid techniques. The multigrid components are modified to work with grids of discrete or continuous functions instead of scalars. For a detailed description of multigrid waveform relaxation see [7, 14, 12]. The multigrid waveform relaxation method is summarised below. The algorithm computes a new approximation  $u^{(\nu+1)}$  starting from a previous approximation  $u^{(\nu)}$ . Barred variables represent quantities on a coarser grid.

- $v \leftarrow u^{(\nu)}$
- **pre-smoothing:** do  $\nu_1$  times {  $v' \leftarrow v$ , solve  $\dot{v} = L^+v + L^-v' + f$  }
- **coarse grid correction:**
  - **calculate defect:**  $d \leftarrow Lv + f - \dot{v}$
  - **solve for coarse grid correction:**  
do  $\gamma$  recursive applications of the algorithm to solve  $\dot{\bar{e}} = \bar{L}\bar{e} + Rd$
  - **correct:**  $v \leftarrow v + P\bar{e}$
- **post-smoothing:** do  $\nu_2$  times {  $v' \leftarrow v$ , solve  $\dot{v} = L^+v + L^-v' + f$  }
- $u^{(\nu+1)} \leftarrow v$

The commonly used V- and W-cycle multigrid methods correspond to  $\gamma = 1$  and  $\gamma = 2$  respectively. On the coarsest grid the solution of the correction equation is usually approximated by applying a few smoothing steps.

### 2.3.2 Coarsening and Smoothing Strategies

Two important components of the multigrid waveform relaxation method are the single-grid waveform relaxation scheme used for smoothing, and the hierarchy of grids used to solve the correction equation. The appropriate choice of these components depends on the properties of the PDE under consideration.

For the *isotropic* diffusion equation point relaxation (e.g., Jacobi, Gauss-Seidel) can be used for smoothing. Standard coarsening can be used to construct a hierarchy of coarser grids. This means that the grid spacing is doubled in both

directions when going to a coarser grid ( $\bar{h} = 2h$ ). Figure 1 shows a set of grids constructed from a fine grid by doubling the grid spacing only in  $x$ , only in  $y$  or in both directions. The grids used for standard coarsening are on the diagonal of Figure 1.

As will be shown by the analysis and numerical results, multigrid waveform relaxation with standard coarsening and a point relaxation method as smoother breaks down for *anisotropic* problems. In this case we need either line relaxation for smoothing or a semicoarsened grid. Experience with the elliptic case suggests the use of the multigrid components given below. Their effectiveness for solving parabolic problems will be illustrated and proven in further sections of this article.

Horizontal *line relaxation* (e.g., horizontal zebra Gauss-Seidel) is expected to do well when there is strong coupling along the  $x$ -direction ( $\varepsilon \gg 1$ ,  $\beta = 0$ ). Conversely vertical line relaxation can be expected to work well for strong coupling along the  $y$ -direction ( $\varepsilon \ll 1$ ,  $\beta = 0$ ). Alternating line relaxation should work in both cases.

Instead of using line relaxation, one can also adapt the coarsening strategy to the anisotropic features of the problem. When there is strong coupling in the  $x$ -direction, one can apply a *semicoarsening* strategy which means that the grid is coarsened only in one direction ( $\bar{h} = (2h_x, h_y)$ ). This correspond to using the grids on the first row of Figure 1. Similarly, one can do semicoarsening in the  $y$ -direction ( $\bar{h} = (h_x, 2h_y)$ ). Multiple semicoarsening methods use all the grids in Figure 1. We consider here the MG-S (multigrid as smoother) method introduced in [16, 15]. One step of this method consists of a multigrid step with standard coarsening where the smoothing has been replaced by semicoarsening in the  $x$ -direction followed by semicoarsening in the  $y$ -direction. This method could also be called alternating semicoarsening. (For Figure 1 the sequence of grids visited would be (2,2), (1,2), (0,2), (1,2), (2,2), (2,1), (2,0), (2,1), (2,2), (1,1), (0,1), (1,1), (1,0), (1,1), (0,0) and back, when using a V-cycle for the standard as well as the semicoarsening steps.)

Full weighting restriction is used to transfer from a fine to a coarse grid. To transfer from a coarse to fine grid linear interpolation is used in the semicoarsening case, and bilinear interpolation is used in the standard coarsening case. See [11] for the details of these operations.

### 3 Fourier-Laplace Analysis

To study the convergence of waveform relaxation methods, we analyse the asymptotic convergence rate of the iteration scheme, which is given by the spectral radius of its iteration operator. We first indicate how the analysis of the time-dependent problem requires the analysis of a stationary problem with a parameter. The latter problem is amenable to classical multigrid analysis.

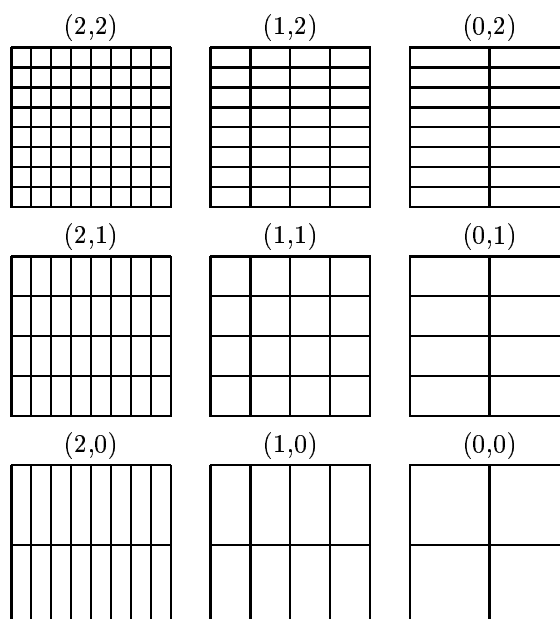


Figure 1: A hierarchy of grids for multilevel methods solving a PDE, discretised on grid  $(92, 2)$ . Standard coarsening uses the grids  $(2, 2)$ ,  $(1, 1)$ ,  $(0, 0)$ . Semi-coarsening in the  $x$ -direction uses the grids  $(2, 2)$ ,  $(1, 2)$ ,  $(0, 2)$ .

### 3.1 Laplace Transform Convergence Analysis of Waveform Relaxation

The relation between the error  $e^{(\nu)} = u - u^{(\nu)}$  of successive waveform relaxation approximations can be written as

$$e^{(\nu+1)} = \mathcal{M}e^{(\nu)}, \quad (10)$$

where  $\mathcal{M}$  is a linear integral operator of Volterra convolution type. In [9, 7, 12, 4, 5] it is shown that the spectral radius of the waveform relaxation operator is given by

$$\rho(\mathcal{M}) = \max_{z \in \Sigma} \rho(M(z)), \quad (11)$$

where  $M(z)$  is the Laplace transform of the convolution kernel of the operator  $\mathcal{M}$ . The set  $\Sigma$  is a subset of the complex plane. Its particular structure depends on the type of waveform method. For the reader's convenience, we recall some results from [12, 4, 5]. For continuous waveform relaxation on a finite time interval,  $\Sigma$  consists of a single point, the point at infinity. For discrete waveform relaxation on a finite time interval, using an LMF for the time discretisation,  $\Sigma$  consists, again, of a single point  $\frac{\alpha_k}{\beta_k} h_t^{-1}$ , with  $\alpha_k$  and  $\beta_k$  parameters of the LMF. For infinite time intervals,  $\Sigma$  is the imaginary axis in the case of continuous time waveform relaxation and the boundary locus of the LMF scaled by  $h_t^{-1}$  for discrete time waveform relaxation. For time-periodic problems  $\Sigma$  consists of a discrete set of points on the imaginary axis or on the scaled boundary locus.

### 3.2 Local Mode Fourier Analysis

In [7, 5, 4] it is shown that the operator  $M(z)$  in (11) is equal to the multigrid iteration operator for solving the discretised linear, stationary PDE  $(zI - L)u = f$ . This system of scalar equations, depending on the parameter  $z$ , can be analysed using standard Fourier analysis [11, 10]. Two-grid analysis assumes one coarser grid on which the correction equation is solved exactly. The iteration operator can then be written as

$$M(z) = S(z)^{\nu_1} K(z) S(z)^{\nu_2}, \quad (12)$$

where  $S(z)$  is the operator of the single-grid waveform relaxation method used as smoother, and  $\nu_1$  and  $\nu_2$  are the number of pre- and post-smoothing steps.  $K(z)$  is the two-grid coarse grid correction operator. It can be written as

$$K(z) = I - P\bar{L}(z)^{-1}RL(z), \quad (13)$$

where  $\bar{L}(z)$  represents the differential operator on the coarse grid, and  $R$  and  $P$  are the restriction and prolongation operators.

The effect of the operator  $M(z)$  on the error can be analysed using Fourier analysis. The error is then decomposed into a sum of exponential Fourier modes of the form

$$\psi(\theta)_{i,j} = \exp(\sqrt{-1}(i\theta_x + j\theta_y)), \quad (14)$$

with

$$\theta \in \Theta_h = \{(\theta_x, \theta_y) \mid \theta_\alpha = 2\pi k_\alpha N_\alpha^{-1}, -\pi \leq \theta_\alpha < \pi, k_\alpha \in \mathbb{Z}, \alpha = x, y\}. \quad (15)$$

The Fourier modes (14) are eigenfunctions of the differential operator  $L$  and of the smoothing operator for the Jacobi method  $S_{\text{Jac}}$ , provided the problem has periodic boundary conditions. It turns out that the convergence factor one obtains using the latter assumption is a good approximation for the case of other boundary conditions as well (Dirichlet, Neumann). Other multigrid operators map an exponential Fourier mode onto a linear combination of related Fourier modes. For each  $\theta \in \Theta'_h = \Theta_h \cap [-\frac{\pi}{2}, \frac{\pi}{2}]^2$ , we define a vector that groups four related Fourier modes (harmonics):

$$\Psi(\theta) = [\psi(\theta^1) \psi(\theta^2) \psi(\theta^3) \psi(\theta^4)]^T, \quad (16)$$

with  $\theta^1 = \theta$  and

$$\theta^2 = \theta - \begin{pmatrix} \text{sign}(\theta_x) \\ \text{sign}(\theta_y) \end{pmatrix} \pi, \quad \theta^3 = \theta - \begin{pmatrix} 0 \\ \text{sign}(\theta_y) \end{pmatrix} \pi, \quad \theta^4 = \theta - \begin{pmatrix} \text{sign}(\theta_x) \\ 0 \end{pmatrix} \pi. \quad (17)$$

The space of grid functions spanned by  $\Psi(\theta)$  is invariant under all the operators considered here. The action of an operator on such a space can be described by a  $4 \times 4$  matrix. This matrix is called the symbol of the operator corresponding to the frequency  $\theta$ . When the exponential Fourier modes are chosen as a basis for representing the errors, the operator  $M(z)$  becomes block triangular with  $4 \times 4$  blocks on the diagonal (the symbols). Therefore, the spectral radius of the

operator  $M(z)$  corresponds to the maximum of the spectral radii of the symbols  $M(z, \theta)$ , and thus

$$\rho(\mathcal{M}) = \max_{z \in \Sigma} \max_{\theta \in \Theta'_h} \rho(M(z, \theta)). \quad (18)$$

In appendix A we summarise the symbols for each of the multigrid components for a general nine-point discretisation.

## 4 Analysis, Results and Discussion

For elliptic anisotropic PDEs robust methods have been developed. We try to establish here whether the conclusions for these methods carry over to the parabolic case. We study three classical model problems: the isotropic diffusion equation ( $\varepsilon = 1, \beta = 0$ ), the anisotropic diffusion equation ( $\varepsilon \in \mathbb{R}, \beta = 0$ ) and the rotated anisotropic diffusion equation ( $\varepsilon \in \mathbb{R}, \beta \in [0, 2\pi)$ ). The equations are discretised on a grid with spacings  $h_x = h_y = 2^{-5}$ . The implicit Euler method (BDF1) with a constant time step  $h_t = 10^{-3}$  ( $N_t = 1000, T = 1$ ) is used as ODE solver. The boundary and initial conditions and the source term  $f$  for (1) are set to 0. This corresponds to a solution  $u = 0$ . For the initial approximation  $u^{(0)}$ , a value chosen from a uniform distribution on  $[-1, 1]$  is assigned to each grid point. The multigrid hierarchy has 5 levels so that the coarsest grid contains one internal point and can be solved by performing 1 smoothing step. In the numerical experiments the convergence factor is estimated by taking the quotient of the norms of the defects after the 20th and 19th iteration.

### 4.1 Diffusion Equation

We first consider the isotropic diffusion equation, an important case both from theoretical and practical point of view. The diffusion equation is given by

$$\frac{\partial u}{\partial t} = \frac{\partial^2 u}{\partial x^2} + \frac{\partial^2 u}{\partial y^2} + f. \quad (19)$$

This corresponds to setting  $\varepsilon = 1$  and  $\beta = 0$  in (2).

Figure 2 illustrates the benefits of multigrid acceleration for this problem. The upper curve shows the norm of the defect for single-grid red-black Gauss-Seidel waveform relaxation. The lower curve shows the norm of the defect on the fine grid for multigrid waveform relaxation. We used a red-black Gauss-Seidel smoother and standard coarsening with a V-cycle using one pre- and one post-smoothing step.

Figure 3 illustrates the Fourier-Laplace analysis graphically. The dashed lines are the scaled boundary loci over which one has to maximise  $\rho(M(z))$  to find  $\rho(\mathcal{M})$  for discrete waveform relaxation on infinite time-intervals (see section 3.1). The contour lines of  $\log_{10} \rho(M(z))$  are represented by solid lines. The infinite interval case is chosen because in practice this gives an accurate approximation of the observed convergence factor [12]. This is motivated by an argument based on pseudospectra in [8, 3]. The numerical results of the analysis will be given in the tables discussed in the next two sections.

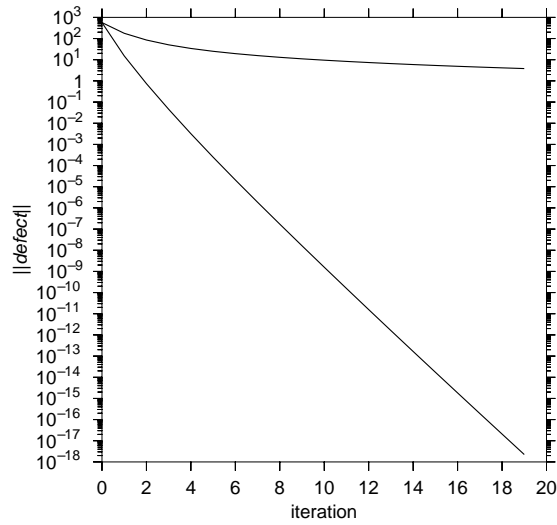


Figure 2: Norm of defect for single-grid waveform relaxation (upper curve, red-black Gauss-Seidel) and multigrid waveform relaxation (lower curve, red-black Gauss-Seidel smoother, full-weighting restriction, bilinear interpolation, V(1,1)-cycle). ( $\varepsilon = 1$ ,  $\beta = 0$ ,  $h = 2^{-5}$ ,  $h_t = 10^{-3}$ ,  $T = 1$ )

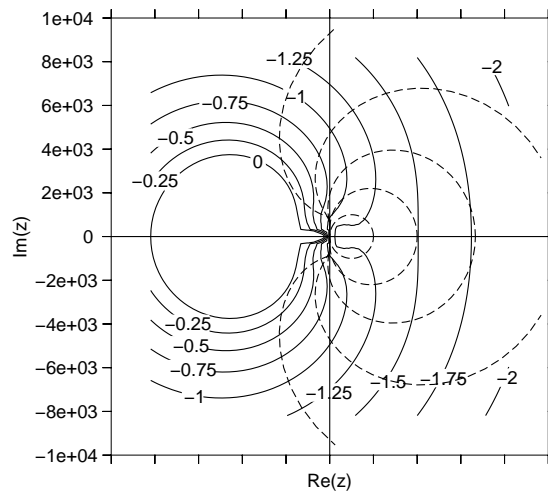


Figure 3: Spectral picture for two-grid waveform relaxation with red-black Gauss-Seidel as smoother and standard coarsening, applied to the discretised isotropic diffusion equation ( $\varepsilon = 1$ ,  $\beta = 0$ ,  $h = 2^{-5}$ ). The solid lines represent contour lines of  $\log_{10}(\rho(M(z)))$ , the dashed lines represent the scaled boundary loci of the BDF1-5 methods ( $h_t = 10^{-3}$ ).

F :	red-black ( $\beta = k\frac{\pi}{2}$ ) or four-colour	S :	standard coarsening
H :	horizontal zebra	X :	$x$ -semicoarsening
V :	vertical zebra	Y :	$y$ -semicoarsening
A :	alternating zebra	A :	alternating semicoarsening

Table 1: Abbreviations used to indicate the smoothing (first column) and coarsening (second column) strategies used. E.g., HY : horizontal zebra Gauss-Seidel with  $y$ -semicoarsening.

## 4.2 Anisotropic Diffusion Equation

As expected from experience with elliptic problems, point relaxation methods are inadequate for solving anisotropic problems. This is confirmed by Figure 4 which shows a spectral picture for an anisotropic problem. The line for  $\rho = 1$  (almost) touches the origin. Therefore (18) will result in convergence factors very close to 1 for  $\Sigma$  sets corresponding to an infinite time interval. Figure 5 shows that when we use vertical zebra Gauss-Seidel as smoother we get a small convergence factor for  $\varepsilon \ll 1$ . The numerical values of the theoretical and observed asymptotic convergence factors can be found in a set of tables given below.

Table 2 illustrates the effect of  $\varepsilon$ . It shows the two-grid theoretical values, the two-grid observed values and the V- and W-cycle results. Large convergence factors are found for  $\varepsilon \neq 1$  (red-black Gauss-Seidel smoothing and standard coarsening). In tables 3 to 6 convergence factors for other combinations of smoothing and coarsening are given. The first column of each table indicates the smoothing and coarsening strategies used (abbreviations are explained in table 1). Table 3 gives the theoretical convergence factor calculated by the two-grid Fourier-Laplace analysis. Table 4 gives convergence factors observed for two-grid waveform relaxation (the correction equation on the coarse grid is approximated by 100 smoothing steps). The observed convergence factors for multigrid waveform relaxation with V- and W-cycles are given in tables 5 and 6. Table 2 compares these four cases for red-black Gauss-Seidel smoothing and standard coarsening. The observed two-grid convergence factors are very close to the theoretical two-grid convergence factor. The W-cycle is, in this case, completely equivalent to the two-grid cycle. In most cases the results for the V-cycle are comparable.

For strong coupling in the  $x$ -direction ( $\varepsilon \gg 1$ ) horizontal zebra Gauss-Seidel with standard coarsening (HS) shows good convergence. The convergence is very bad, however for strong coupling in the  $y$ -direction ( $\varepsilon \ll 1$ ). The converse is true when we use vertical zebra Gauss-Seidel as smoother. Combining these two methods into alternating zebra Gauss-Seidel results in good convergence for all values of  $\varepsilon$ . These results confirm the findings for the stationary multigrid case.

The results of the Fourier-Laplace analysis in table 3 indicate that we could expect similar results for red-black Gauss-Seidel smoothing with  $x$ - and  $y$ -semicoarsening (FX, FY). The numerical results in table 5, however, show poor convergence for moderate values of  $\varepsilon$ . The two-grid Fourier-Laplace analysis assumes that the correction equation on the coarse grid is solved exactly or nearly so. In the V- and W-cycle case, this assumption is not satisfied, because through

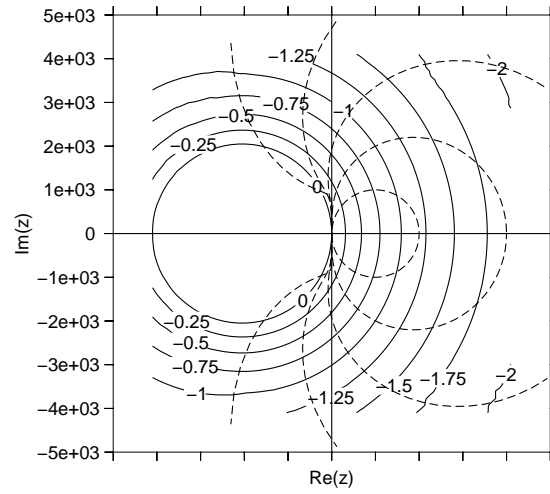


Figure 4: Spectral picture for two-grid waveform relaxation with red-black Gauss-Seidel as smoother and standard coarsening, applied to the discretised anisotropic diffusion equation. ( $\varepsilon = 10^{-3}$ ,  $\beta = 0$ ,  $h = 2^{-5}$ ) The solid lines represent contour lines of  $\log_{10}(\rho(M(z)))$ , the dashed lines represent the scaled boundary loci of BDF1 to BDF5 ( $h_t = 10^{-3}$ ).

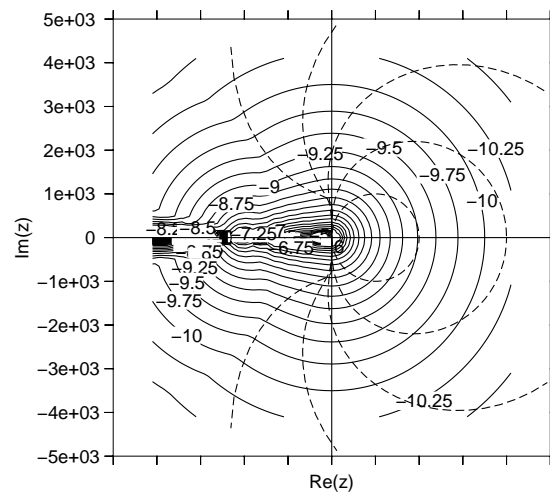


Figure 5: Spectral picture for two-grid waveform relaxation with vertical zebra Gauss-Seidel as smoother and standard coarsening, applied to the discretised anisotropic diffusion equation. ( $\varepsilon = 10^{-3}$ ,  $\beta = 0$ ,  $h = 2^{-5}$ ) The solid lines represent contour lines of  $\log_{10}(\rho(M(z)))$ , the dashed lines represent the scaled boundary loci of BDF1 to BDF5 ( $h_t = 10^{-3}$ ).

	$\varepsilon$	$10^{-4}$	$10^{-3}$	$10^{-2}$	$10^{-1}$	$2^{-1}$	1	2	$10^1$	$10^2$	$10^3$	$10^4$
two-grid, theoretical	0.994	0.990	0.956	0.680	0.197	0.075	0.197	0.683	0.961	0.996	1.000	
V-cycle, numerical	0.936	0.931	0.890	0.648	0.210	0.108	0.209	0.649	0.898	0.937	0.937	
W-cycle, numerical	0.936	0.931	0.890	0.646	0.188	0.072	0.188	0.647	0.898	0.937	0.937	
two-grid, numerical	0.936	0.931	0.890	0.646	0.188	0.072	0.188	0.647	0.898	0.938	0.937	

Table 2: Convergence factors for waveform relaxation with red-black Gauss-Seidel and standard coarsening, applied to the anisotropic diffusion equation. ( $\beta = 0$ ,  $h = 2^{-5}$ ,  $h_t = 10^{-3}$ , BDF1)

$\varepsilon$	$10^{-4}$	$10^{-3}$	$10^{-2}$	$10^{-1}$	$2^{-1}$	1	2	$10^1$	$10^2$	$10^3$	$10^4$
FS	0.994	0.990	0.956	0.680	0.197	0.075	0.197	0.683	0.961	0.996	1.000
HS	0.994	0.990	0.956	0.680	0.197	0.093	0.093	0.093	0.093	0.093	0.093
VS	$\sim 10^{-7}$	$\sim 10^{-4}$	0.014	0.145	0.114	0.093	0.197	0.683	0.961	0.996	1.000
AS	$\sim 10^{-7}$	$\sim 10^{-4}$	0.013	0.110	0.043	0.029	0.034	0.070	0.090	0.093	0.093
FX	0.994	0.990	0.956	0.680	0.197	0.072	0.061	0.053	0.013	0.001	$\sim 10^{-3}$
FY	0.093	0.093	0.093	0.090	0.080	0.072	0.197	0.683	0.961	0.996	1.000
FA	0.004	0.004	0.004	0.001	$\sim 10^{-4}$	$\sim 10^{-5}$	$\sim 10^{-4}$	$\sim 10^{-3}$	$\sim 10^{-3}$	$\sim 10^{-5}$	$\sim 10^{-7}$
HY	0.093	0.093	0.093	0.093	0.093	0.093	0.093	0.093	0.093	0.093	0.093
VX	$\sim 10^{-7}$	$\sim 10^{-4}$	0.014	0.145	0.114	0.093	0.072	0.053	0.013	0.001	$\sim 10^{-3}$

Table 3: *Theoretical* convergence factors for *two-grid* waveform relaxation with different combinations of smoothing and coarsening strategies, applied to the anisotropic diffusion equation. ( $\beta = 0$ ,  $h = 2^{-5}$ ,  $h_t = 10^{-3}$ , BDF1, infinite time interval)

grid stretching semicoarsening introduces an anisotropy that is strongly increasing with growing number of grid levels (see remark 5.1.3 on p. 134 of [11]). We can therefore expect the multigrid method to fail on the coarser grids, which renders the two-grid approximation invalid. From the numerical results for V- and W-cycles it becomes clear that the semicoarsening methods only work for very specific values of  $\varepsilon$ . The alternating semicoarsening method with red-black Gauss-Seidel as smoother (FA), however, shows very good convergence for all values of  $\varepsilon$ . Combination of a smoother that works well for coupling in one direction with semicoarsening for the other direction results in robust solvers as well (rows HY and VX). These results confirm the results obtained for the stationary multigrid case. Table 7 summarises our findings.

### 4.3 Rotated Anisotropic Diffusion Equation

The previous results show that good convergence can be obtained for problems with strong coupling in the direction of the coordinate axes. The tables 8, 9 and 10 show convergence factors for different methods as a function of the angle  $\beta$ , with fixed  $\varepsilon = 10^{-3}$ . Because of symmetry it is sufficient to consider  $\beta \in [0, \frac{\pi}{2})$ . We can conclude that all of the methods considered here have problems when the coupling is not aligned with the grid. Similar results are obtained for  $\varepsilon \gg 1$ . Again the result observed for the V-cycle is worse than expected from the two-grid Fourier-Laplace analysis. The W-cycle results are closer to the theoretical two-grid ones. The results for different smoothers and

$\varepsilon$	$10^{-4}$	$10^{-3}$	$10^{-2}$	$10^{-1}$	$2^{-1}$	1	2	$10^1$	$10^2$	$10^3$	$10^4$
FS	0.936	0.931	0.890	0.646	0.188	0.072	0.188	0.647	0.898	0.938	0.937
HS	0.936	0.931	0.889	0.646	0.188	0.087	0.086	0.079	0.048	0.002	$\sim 10^{-5}$
VS	$\sim 10^{-7}$	$\sim 10^{-4}$	0.040	0.120	0.106	0.086	0.188	0.647	0.898	0.938	0.937
AS	$\sim 10^{-7}$	$\sim 10^{-4}$	0.021	0.091	0.046	0.042	0.031	0.058	0.046	0.002	$\sim 10^{-5}$
FX	0.936	0.932	0.891	0.646	0.188	0.077	0.023	0.050	0.022	0.020	0.020
FY	0.089	0.089	0.088	0.085	0.076	0.023	0.250	0.647	0.900	0.938	0.937
FA	0.004	0.004	0.003	0.001	$\sim 10^{-4}$	$\sim 10^{-5}$	$\sim 10^{-4}$	$\sim 10^{-3}$	$\sim 10^{-4}$	$\sim 10^{-4}$	$\sim 10^{-3}$
HY	0.089	0.089	0.088	0.088	0.087	0.038	0.216	0.276	0.049	$\sim 10^{-3}$	$\sim 10^{-5}$
VX	$\sim 10^{-7}$	$\sim 10^{-4}$	0.037	0.117	0.065	0.027	0.026	0.050	0.023	0.020	0.020

Table 4: *Numerically observed* convergence factors for *two-grid* waveform relaxation with different combinations of smoothing and coarsening strategies, applied to the anisotropic diffusion equation. ( $\beta = 0$ ,  $h = 2^{-5}$ ,  $h_t = 10^{-3}$ , BDF1)

$\varepsilon$	$10^{-4}$	$10^{-3}$	$10^{-2}$	$10^{-1}$	$2^{-1}$	1	2	$10^1$	$10^2$	$10^3$	$10^4$
FS	0.936	0.931	0.890	0.648	0.210	0.108	0.209	0.649	0.898	0.937	0.937
HS	0.936	0.931	0.889	0.648	0.197	0.110	0.106	0.086	0.053	0.002	$\sim 10^{-5}$
VS	$\sim 10^{-7}$	$\sim 10^{-4}$	0.036	0.108	0.113	0.110	0.196	0.649	0.898	0.937	0.937
AS	$\sim 10^{-7}$	$\sim 10^{-4}$	0.020	0.085	0.053	0.052	0.040	0.057	0.050	0.002	$\sim 10^{-5}$
FX	0.935	0.930	0.895	0.868	0.863	0.852	0.821	0.659	0.237	0.036	0.004
FY	0.116	0.115	0.129	0.654	0.822	0.852	0.860	0.867	0.902	0.938	0.937
FA	0.011	0.011	0.009	0.004	0.035	0.034	0.030	0.011	0.003	$\sim 10^{-3}$	$\sim 10^{-4}$
HY	0.116	0.115	0.114	0.114	0.113	0.111	0.108	0.090	0.054	0.002	$\sim 10^{-5}$
VX	$\sim 10^{-7}$	$\sim 10^{-4}$	0.036	0.108	0.115	0.112	0.101	0.168	0.123	0.018	$\sim 10^{-3}$

Table 5: *Numerically observed* convergence factors for *multigrid* waveform relaxation with different combinations of smoothing and coarsening strategies, applied to the anisotropic diffusion equation. ( $\beta = 0$ ,  $h = 2^{-5}$ ,  $h_t = 10^{-3}$ , BDF1, *V-cycle*)

$\varepsilon$	$10^{-4}$	$10^{-3}$	$10^{-2}$	$10^{-1}$	$2^{-1}$	1	2	$10^1$	$10^2$	$10^3$	$10^4$
FS	0.936	0.931	0.890	0.646	0.188	0.072	0.188	0.647	0.898	0.937	0.937
HS	0.936	0.931	0.889	0.646	0.188	0.088	0.087	0.080	0.048	0.002	$\sim 10^{-5}$
VS	$\sim 10^{-7}$	$\sim 10^{-4}$	0.040	0.120	0.106	0.088	0.188	0.647	0.898	0.938	0.937
AS	$\sim 10^{-7}$	$\sim 10^{-4}$	0.021	0.091	0.046	0.042	0.030	0.058	0.045	0.002	$\sim 10^{-5}$
FX	0.936	0.931	0.890	0.704	0.571	0.480	0.369	0.050	0.010	$\sim 10^{-3}$	$\sim 10^{-4}$
FY	0.091	0.090	0.089	0.088	0.038	0.485	0.569	0.707	0.900	0.938	0.937
FA	0.005	0.004	0.004	0.001	$\sim 10^{-4}$	$\sim 10^{-5}$	$\sim 10^{-4}$	$\sim 10^{-3}$	$\sim 10^{-4}$	$\sim 10^{-6}$	$\sim 10^{-8}$
HY	0.091	0.090	0.089	0.089	0.089	0.089	0.088	0.081	0.048	0.002	$\sim 10^{-5}$
VX	$\sim 10^{-7}$	$\sim 10^{-4}$	0.040	0.121	0.106	0.088	0.069	0.049	0.010	$\sim 10^{-3}$	$\sim 10^{-5}$

Table 6: *Numerically observed* convergence factors for *multigrid* waveform relaxation with different combinations of smoothing and coarsening strategies, applied to the anisotropic diffusion equation. ( $\beta = 0$ ,  $h = 2^{-5}$ ,  $h_t = 10^{-3}$ , BDF1, *W-cycle*)

	FS	HS	VS	AS	FX	FY	FA	HY	VX
$\varepsilon \ll 1$	-	-	+	+	-	$\pm$	+	+	+
$\varepsilon \gg 1$	-	+	-	+	$\pm$	-	+	+	+

Table 7: Performance of multigrid waveform relaxation applied to the anisotropic diffusion equation.

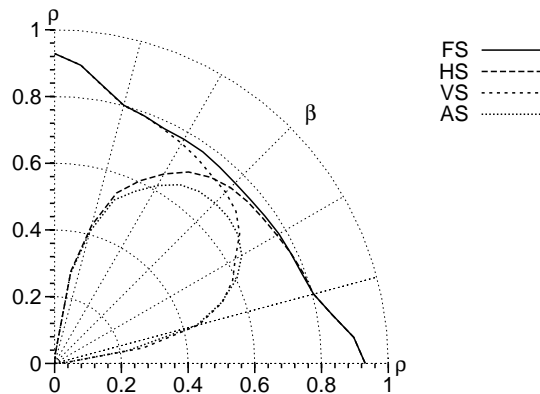


Figure 6: Polar plot  $(\rho, \beta)$  of *numerically observed* convergence factors for *multigrid* waveform relaxation with different smoothers and standard coarsening, applied to the rotated anisotropic diffusion equation. ( $\varepsilon = 10^{-3}$ ,  $h = 2^{-5}$ ,  $h_t = 10^{-3}$ , BDF1, *V-cycle*)

standard coarsening with a V-cycle are graphically illustrated in Figure 6. In this polar plot the convergence factor  $\rho$  is plotted in function of the direction  $\beta$  of the anisotropy. A circular curve with a small radius would indicate a robust method.

If the direction of coupling is unknown, it is best to use a method with good convergence for all values of  $\varepsilon$  in the non-rotated anisotropic case. It may be necessary, however, to consider other methods like incomplete LU factorisation smoothing when strong non-alignment can occur.

#### 4.4 Example Problem with Variable Coefficients

We illustrate the results with the more general linear equation

$$\frac{\partial u}{\partial t} = \frac{\partial}{\partial x} \left( a \frac{\partial u}{\partial x} \right) + \frac{\partial}{\partial y} \left( b \frac{\partial u}{\partial y} \right) + f \quad (20)$$

with variable coefficients  $a(x, y) = e^{10(x-y)}$  and  $b(x, y) = e^{-10(x-y)}$ . This problem has strong coupling in both directions. The initial conditions, Dirichlet boundary conditions and source term  $f$  are chosen such that the exact solution is  $u(t, x, y) = t + x + y$ . In table 11 the convergence factors are given for multigrid waveform relaxation methods with different combination of smoothing and coarsening strategies. As expected only the robust methods (AS, FA, HY, VX) show good convergence. The same discretisation as before is used

$\beta$	0°	15°	30°	45°	60°	75°	90°
FS	0.990	0.788	0.682	0.664	0.683	0.788	0.990
HS	0.990	0.788	0.667	0.611	0.541	0.335	$\sim 10^{-4}$
VS	$\sim 10^{-4}$	0.335	0.541	0.611	0.667	0.788	0.990
AS	$\sim 10^{-4}$	0.312	0.486	0.532	0.486	0.312	$\sim 10^{-4}$
FX	0.990	0.788	0.634	0.528	0.366	0.144	0.093
FY	0.093	0.144	0.364	0.530	0.637	0.788	0.990
FA	0.004	0.009	0.045	0.061	0.040	0.007	0.004
HY	0.093	0.162	0.354	0.479	0.493	0.330	$\sim 10^{-4}$
VX	$\sim 10^{-4}$	0.330	0.493	0.479	0.354	0.162	0.093

Table 8: *Theoretical* convergence factors for *two-grid* waveform relaxation with different combinations of smoothing and coarsening strategies applied to the rotated anisotropic diffusion equation. ( $\varepsilon = 10^{-3}$ ,  $h = 2^{-5}$ ,  $h_t = 10^{-3}$ , BDF1, infinite time interval)

$\beta$	0°	15°	30°	45°	60°	75°	90°
FS	0.931	0.804	0.776	0.765	0.775	0.801	0.928
HS	0.931	0.804	0.769	0.745	0.656	0.428	$\sim 10^{-4}$
VS	$\sim 10^{-4}$	0.448	0.625	0.725	0.761	0.800	0.929
AS	$\sim 10^{-4}$	0.440	0.648	0.680	0.616	0.410	$\sim 10^{-4}$
FX	0.930	0.897	0.883	0.877	0.815	0.578	0.115
FY	0.115	0.625	0.816	0.874	0.889	0.892	0.928
FA	0.011	0.111	0.294	0.370	0.328	0.102	0.011
HY	0.115	0.472	0.658	0.685	0.625	0.415	$\sim 10^{-4}$
VX	$\sim 10^{-4}$	0.441	0.604	0.667	0.633	0.492	0.115

Table 9: *Numerically observed* convergence factors for *multigrid* waveform relaxation with different combinations of smoothing and coarsening strategies applied to the rotated anisotropic diffusion equation. ( $\varepsilon = 10^{-3}$ ,  $h = 2^{-5}$ ,  $h_t = 10^{-3}$ , BDF1, *V-cycle*)

$\beta$	0°	15°	30°	45°	60°	75°	90°
FS	0.931	0.766	0.697	0.688	0.696	0.767	0.929
HS	0.931	0.767	0.689	0.659	0.583	0.409	$\sim 10^{-4}$
VS	$\sim 10^{-4}$	0.410	0.571	0.648	0.686	0.766	0.929
AS	$\sim 10^{-4}$	0.422	0.582	0.606	0.555	0.398	$\sim 10^{-4}$
FX	0.931	0.853	0.799	0.732	0.585	0.232	0.090
FY	0.090	0.218	0.585	0.745	0.813	0.850	0.929
FA	0.004	0.020	0.119	0.162	0.100	0.017	0.004
HY	0.090	0.227	0.458	0.553	0.539	0.396	$\sim 10^{-4}$
VX	$\sim 10^{-4}$	0.399	0.533	0.542	0.466	0.226	0.090

Table 10: *Numerically observed* convergence factors for *multigrid* waveform relaxation with different combinations of smoothing and coarsening strategies applied to the rotated anisotropic diffusion equation ( $\varepsilon = 10^{-3}$ ,  $h = 2^{-5}$ ,  $h_t = 10^{-3}$ , BDF1, *W-cycle*).

FS	HS	VS	FX	FY
0.9207(>177)	0.9209(>178)	0.8926(>121)	0.8876(>121)	0.8867(>115)
AS	HY	VX	FA	
0.0175(3)	0.1009(8)	0.1166(8)	0.0073(4)	

Table 11: Numerically observed convergence factors for multigrid waveform relaxation applied to (20). Number of iteration needed for reduction of norm of defect by  $10^{-8}$  between brackets. ( $h = 2^{-5}$ ,  $h_t = 10^{-3}$ , BDF1)

( $h_x = h_y = 2^{-5}$ , 5 levels,  $h_t = 10^{-3}$ , BDF1), together with V-cycles with one pre- and one post-smoothing step. The number between brackets indicates the number of iterations needed to get a reduction of the norm of the defect by a factor  $10^{-8}$ . At this point precision up to discretisation error was reached for all the converging methods. The convergence factor is estimated by the quotient of the norms of the defect in the last and second to last iteration. If more than 20 iterations were needed the convergence factor was estimated using the norm of the defect in the 19th and 20th iteration. This value is then used to estimate the expected number of iterations.

#### 4.5 Correction for Computational Complexity

Obviously a multigrid iteration is more expensive than a single-grid iteration. Similarly line relaxation and semicoarsening are more expensive than point relaxation. To fairly compare the different methods we should introduce a convergence factor relative to the amount of work needed for one iteration. As a “work unit” one usually takes the amount of work needed to do one single-grid point relaxation on the finest grid.

The tridiagonal systems that have to be solved for line relaxation involve approximately double the amount of work of point relaxation. The amount of work is also proportional to the number of smoothing steps ( $\nu_1 + \nu_2$ ). For the different coarsening strategies we can estimate the amount of work by counting the number of points visited. For V-cycles this results in the factors given in table 12. We can now estimate, for example, that one multigrid waveform iteration with point relaxation and alternating semicoarsening with V(1,1)-cycles takes approximately  $10\frac{2}{3}$  work units. For a method that has a convergence factor  $\rho$ , and takes  $\alpha$  work units per iteration, the convergence factor per work unit is equal to  $\tilde{\rho} = \sqrt[\alpha]{\rho}$ . Figure 7 compares the corrected convergence factor for the standard coarsening multigrid waveform relaxation methods, applied to the anisotropic model problem ( $\beta = 0$ ). The FS, VS and HS methods all have a parameter region where they work best and another region where they perform (very) poorly. The computationally expensive AS method works well over the entire parameter region. This behaviour is typical also for the rotated problem and for other multigrid operator combinations.

Point Relaxation	$\nu_1 + \nu_2$	Standard Coarsening	$\frac{4}{3}$
Line Relaxation	$2(\nu_1 + \nu_2)$	Semicoarsening	2
		Alternating Semicoarsening	$\frac{16}{3}$

Table 12: Correction factors for different smoothing and coarsening strategies (V-cycle)

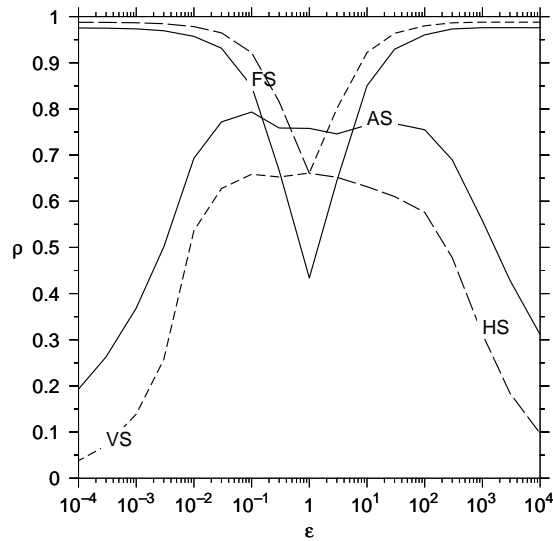


Figure 7: Numerically observed convergence factors “per work unit” for *multigrid* waveform relaxation with different smoothers and standard coarsening, applied to the anisotropic diffusion equation. ( $\beta = 0$ ,  $h = 2^{-5}$ ,  $h_t = 10^{-3}$ , BDF1, *V-cycle*)

## 5 Conclusions

We have shown that it is possible to extend the multigrid methods developed for stationary anisotropic problems to multigrid waveform relaxation methods for the corresponding time-dependent problems. The convergence rates are qualitatively similar for the stationary and the time-dependent methods. For problems where the anisotropy is aligned to the grid, alternating line relaxation with standard coarsening and point relaxation with alternating semicoarsening are appropriate methods. These methods are still useful for problems where the anisotropy is not aligned with the grid, but the performance is not optimal anymore. The performance of any method may strongly depend on the particular parameter values, and needs to be corrected for its computational complexity.

## A Symbols of Standard Multigrid Components

In this section we summarise the symbols of the multigrid components for discretisations using the nine-point stencil

$$\begin{bmatrix} s_{-1,1} & s_{0,1} & s_{1,1} \\ s_{-1,0} & s_{0,0} & s_{1,0} \\ s_{-1,-1} & s_{0,-1} & s_{1,-1} \end{bmatrix}. \quad (21)$$

For their derivation we have followed [17, 11]. We introduce the following notation.

$$C(z) = z - s_{0,0} \quad (22)$$

$$H(\theta) = -s_{1,0} \exp(i\theta_x) - s_{-1,0} \exp(-i\theta_x) \quad (23)$$

$$V(\theta) = -s_{0,1} \exp(i\theta_y) - s_{0,-1} \exp(-i\theta_y) \quad (24)$$

$$D(\theta) = -s_{1,1} \exp(i(\theta_x + \theta_y)) - s_{1,-1} \exp(i(\theta_x - \theta_y)) - s_{-1,-1} \exp(i(-\theta_x - \theta_y)) - s_{-1,1} \exp(i(-\theta_x + \theta_y)) \quad (25)$$

The following relations can be used to simplify the calculations.

$$\begin{aligned} H(\theta^1) &= -H(\theta^2) &= H(\theta^3) &= -H(\theta^4) \\ V(\theta^1) &= -V(\theta^2) &= -V(\theta^3) &= V(\theta^4) \\ D(\theta^1) &= D(\theta^2) &= -D(\theta^3) &= -D(\theta^4) \end{aligned} \quad (26)$$

We recall that the multigrid symbol is given by

$$M(z, \theta) = S(z, \theta)^{\nu_1} K(z, \theta) S(z, \theta)^{\nu_2}, \quad (27)$$

where the two-grid coarse grid correction symbol  $K(z, \theta)$  involves the symbols of the differential operator on the fine and the coarse grid and the symbols of the restriction and prolongation operators.

### A.1 Differential Operator

The exponential Fourier modes (14) are eigenvalues of the differential operator, leading to a diagonal matrix as the symbol for  $L$  :

$$L(z, \theta) = \begin{bmatrix} \tilde{L}(z, \theta^1) & & & \\ & \tilde{L}(z, \theta^2) & & \\ & & \tilde{L}(z, \theta^3) & \\ & & & \tilde{L}(z, \theta^4) \end{bmatrix}, \quad (28)$$

$$\tilde{L}(z, \theta) = C(z) + H(\theta) + V(\theta) + D(\theta). \quad (29)$$

### A.2 Smoothing Operator

For a general nine-point discretisation, the symbol of the smoothing operators considered in this paper can be written as

$$S(z, \theta) = T^{-1}(T \cdot A(z, \theta)), \quad (30)$$

where  $T \cdot A$  denotes point-wise multiplication and with  $A(z, \theta)$  and  $T$  given by

$$A(z, \theta) = \begin{bmatrix} \alpha_{00}(z, \theta^1) & \alpha_{00}(z, \theta^2) & \alpha_{00}(z, \theta^3) & \alpha_{00}(z, \theta^4) \\ \alpha_{11}(z, \theta^1) & \alpha_{11}(z, \theta^2) & \alpha_{11}(z, \theta^3) & \alpha_{11}(z, \theta^4) \\ \alpha_{01}(z, \theta^1) & \alpha_{01}(z, \theta^2) & \alpha_{01}(z, \theta^3) & \alpha_{01}(z, \theta^4) \\ \alpha_{10}(z, \theta^1) & \alpha_{10}(z, \theta^2) & \alpha_{10}(z, \theta^3) & \alpha_{10}(z, \theta^4) \end{bmatrix}, \quad (31)$$

$$T = \begin{bmatrix} 1 & 1 & 1 & 1 \\ 1 & 1 & -1 & -1 \\ 1 & -1 & -1 & 1 \\ 1 & -1 & 1 & -1 \end{bmatrix}. \quad (32)$$

The matrix elements  $\alpha_{..}(z, \theta)$  depend on the particular smoothing scheme, and are given below for the smoothers considered here.

#### Red-Black Gauss-Seidel

$$\begin{cases} \alpha_{11}(z, \theta) = \alpha_{00}(z, \theta) = -(H(\theta) + V(\theta))/C(z) \\ \alpha_{10}(z, \theta) = \alpha_{01}(z, \theta) = \alpha_{11}(z, \theta)^2 \end{cases} \quad (33)$$

#### Four-Colour Gauss-Seidel

$$\begin{cases} \alpha_{11}(z, \theta) = -(H(\theta) + V(\theta) + D(\theta))/C(z) \\ \alpha_{00}(z, \theta) = -(H(\theta) + V(\theta) + \alpha_{11}(z, \theta)D(\theta))/C(z) \\ \alpha_{01}(z, \theta) = -(\alpha_{11}H(\theta) + \alpha_{00}(z, \theta)V(\theta) + D(\theta))/C(z) \\ \alpha_{10}(z, \theta) = -(\alpha_{00}H(\theta) + \alpha_{11}(z, \theta)V(\theta) + \alpha_{01}(z, \theta)D(\theta))/C(z) \end{cases} \quad (34)$$

#### Horizontal Zebra Gauss-Seidel

$$\begin{cases} \alpha_{11}(z, \theta) = \alpha_{01}(z, \theta) = -(V(\theta) + D(\theta))/(C(z) + H(\theta)) \\ \alpha_{10}(z, \theta) = \alpha_{00}(z, \theta) = \alpha_{11}(z, \theta)^2 \end{cases} \quad (35)$$

### Vertical Zebra Gauss-Seidel

$$\begin{cases} \alpha_{11}(z, \theta) = \alpha_{10}(z, \theta) = -(H(\theta) + D(\theta))/(C(z) + V(\theta)) \\ \alpha_{01}(z, \theta) = \alpha_{00}(z, \theta) = \alpha_{11}(z, \theta)^2 \end{cases} \quad (36)$$

### Alternating Zebra Gauss-Seidel

The symbol for this smoother can be found as the product of the symbols for the vertical and horizontal zebra Gauss-Seidel methods. We follow [17] and use an alternative vertical zebra method where the lines with even  $i$  are updated first. This yields slightly improved convergence and more symmetric results. The symbol for this alternative operator can be found by interchanging  $\alpha_{11}$  and  $\alpha_{10}$  with  $\alpha_{00}$  and  $\alpha_{01}$  in (36).

### A.3 Coarse Grid Correction Operator

In this paper full-weighting restriction and (bi)linear interpolation are considered. The symbol of the prolongation (interpolation) operator is the transpose of the symbol of the restriction operator,

$$P(\theta) = R(\theta)^T. \quad (37)$$

The symbol of the two-grid coarse grid correction operator is given by

$$K(z, \theta) = I - P(\theta)\bar{L}(z, \bar{\theta})^{-1}R(\theta)L(z, \theta). \quad (38)$$

The operator  $K(z, \theta)$  depends on the coarsening strategy used, and is specified for standard, semicoarsening and multiple semicoarsening in the following sections.  $\bar{L}(z, \theta)$  is the symbol of the operator corresponding to the stencil on the coarse grid ( $h$  is replaced by  $\bar{h}$ ).

#### A.3.1 Standard Coarsening, $\bar{h} = 2h$ , $\bar{\theta} = 2\theta$

$$\bar{L} = \left[ \tilde{\tilde{L}}(\bar{\theta}^1) \right] \quad (39)$$

$$R(\theta) = \left[ \tilde{R}(\theta^1) \quad \tilde{R}(\theta^2) \quad \tilde{R}(\theta^3) \quad \tilde{R}(\theta^4) \right] \quad (40)$$

$$\tilde{R}(\theta) = \frac{1}{4}(1 + \cos(\theta_x))(1 + \cos(\theta_y)) \quad (41)$$

#### A.3.2 $x$ -semicoarsening, $\bar{h} = (2h_x, h_y)$ , $\bar{\theta} = (2\theta_x, \theta_y)$

$$\bar{L} = \left[ \begin{array}{c} \tilde{\tilde{L}}(\bar{\theta}^1) \\ \tilde{\tilde{L}}(\bar{\theta}^3) \end{array} \right] \quad (42)$$

$$R(\theta) = \left[ \begin{array}{cccc} \tilde{R}(\theta^1) & 0 & 0 & \tilde{R}(\theta^4) \\ 0 & \tilde{R}(\theta^2) & \tilde{R}(\theta^3) & 0 \end{array} \right] \text{ with } \tilde{R}(\theta) = \frac{1}{2}(1 + \cos(\theta_x)) \quad (43)$$

**A.3.3  $y$ -semicoarsening,**  $\bar{h} = (h_x, 2h_y)$ ,  $\bar{\theta} = (\theta_x, 2\theta_y)$

$$\bar{L} = \begin{bmatrix} \tilde{\tilde{L}}(\bar{\theta}^1) & \\ & \tilde{\tilde{L}}(\bar{\theta}^4) \end{bmatrix} \quad (44)$$

$$R(\theta) = \begin{bmatrix} \tilde{R}(\theta) & 0 & \tilde{R}(\theta^3) & 0 \\ 0 & \tilde{R}(\theta^2) & 0 & \tilde{R}(\theta^4) \end{bmatrix} \text{ with } \tilde{R}(\theta) = \frac{1}{2}(1 + \cos(\theta_y)) \quad (45)$$

### A.3.4 Multiple Semicoarsening

Multiple semicoarsening uses a two-dimensional hierarchy of grids as illustrated in Figure 1. The smoothing step is replaced by an  $x$ -semicoarsening step followed by an  $y$ -semicoarsening step. We now use three coarser grids for the analysis instead of one: one corresponding to each of the semicoarsening steps and one for the standard coarsening step. The multigrid operator (and the corresponding symbol) can be written as follows

$$\begin{aligned} M &= (M_x M_y)^{\nu_1} K (M_x M_y)^{\nu_2}, \\ M_x &= S^{\mu_1} K_x S^{\mu_2}, \quad M_y = S^{\mu_1} K_y S^{\mu_2}, \end{aligned} \quad (46)$$

where  $M_x$  and  $M_y$  are the semicoarsening multigrid operators (symbols) and  $K_x$  and  $K_y$  are the corresponding semicoarsening coarse grid correction operators.

## References

- [1] K. Burrage. *Parallel and Sequential Methods for Ordinary Differential Equations*. Oxford University Press, Oxford, 1995.
- [2] G. Horton and S. Vandewalle. A space-time multigrid method for parabolic partial differential equations. *SIAM J. Sci. Comp.*, 16(4):848–864, July 1995.
- [3] Z. Jackiewicz, B. Owren, and B. Welfert. Convergence analysis of waveform relaxation methods using pseudospectra. submitted.
- [4] J. Janssen and S. Vandewalle. Multigrid waveform relaxation on spatial finite element meshes: the continuous-time case. *SIAM J. Numer. Anal.*, 33(2):456–474, April 1996.
- [5] J. Janssen and S. Vandewalle. Multigrid waveform relaxation on spatial finite element meshes: the discrete-time case. *SIAM J. Sci. Comp.*, 17(1):135–155, January 1996.
- [6] E. Lelarasmee, A. E. Ruehli, and A. L. Sangiovanni-Vincentelli. The waveform relaxation method for time-domain analysis of large scale integrated circuits. *IEEE Trans. on CAD of IC Sys.*, 1:131–145, 1982.
- [7] C. Lubich and A. Ostermann. Multigrid dynamic iteration for parabolic equations. *BIT*, 27:216–234, 1987.
- [8] A. Lumsdaine and D. Wu. Spectra and pseudospectra of waveform relaxation operators. *SIAM J. Sci. Comp.*, 18(1):286–304, 1997.

- [9] U. Mikkala and O. Nevanlinna. Convergence of dynamic iteration methods for initial value problems. *SIAM J. Sci. Stat. Comp.*, 8:459–482, 1997.
- [10] S. Ta’asan and H. Zhang. On the multigrid waveform relaxation method. *SIAM J. Sci. Comp.*, 16(5):1092–1104, September 1995.
- [11] U. Trottenberg, C. W. Oosterlee, and A. Schüller. *Multigrid methods*. Academic Press, 2000.
- [12] S. Vandewalle. *Parallel multigrid waveform relaxation for parabolic problems*. B. G. Teubner, Stuttgart, 1993.
- [13] S. Vandewalle and G. Horton. Fourier mode analysis of the multigrid waveform relaxation and time-parallel multigrid methods. *Computing*, 54:317–330, 1995.
- [14] S. Vandewalle and R. Piessens. Efficient parallel algorithms for solving initial-boundary and time-periodic parabolic partial differential equations. *SIAM J. Sci. Stat. Comp.*, 13(6):1330–1346, November 1992.
- [15] T. Washio and C. W. Oosterlee. On the robustness of a multiple semicoarsened grid method. *Z. angew. Math. Mech.*, 75(4):251–257, 1995.
- [16] T. Washio and C. W. Oosterlee. Flexible multiple semicoarsening for three-dimensional singularly perturbed problems. *SIAM J. Sci. Comp.*, 19(5):1646–1666, September 1998.
- [17] P. Wesseling. *An introduction to multigrid methods*. John Wiley & Sons, Chichester, 1992.